

# A comparison of different connection techniques for thermoelectric generators in vehicle waste heat recovery



---

**Björn Andersson**

Division of Industrial Electrical Engineering and Automation  
Faculty of Engineering, Lund University



LUND UNIVERSITY



# A comparison of different connection techniques for thermoelectric generators in vehicle waste heat recovery

Degree Project in Industrial Electrical Engineering and Automation, EIE920

*Author:* Björn Andersson  
October 2012

Supervisor Scania: Jan Dellrud  
Supervisor IEA: Avo Reinap  
Examiner: Mats Alaküla

# Abstract

Increasing demand for lower fuel consumption increases the importance of a higher total energy efficiency in trucks. Since the efficiency of a modern diesel engine is in the range of 40 %, large amounts of waste heat are produced.

Recovering this energy can be done with thermoelectric generators. However, these generators' open load voltage and internal resistance are temperature dependant, which results in different optimal output currents for different working conditions according to the maximum power transfer theorem.

Connecting the thermoelectric generators to a DC/DC-converter using Maximum Power Point Tracking (MPPT) technology can aid in this matter, as can switching between different serial and parallel configurations.

In this project, the recovery potential of several different connection techniques for test rig with a power output of tens of watts is presented.

It is shown that a switching network may allow more energy to be recovered than when using a DC/DC-converter. However, further investigations are needed to determine which solution is more suitable for TEG-rigs with output powers in the kW-range.

The results show that a switching network with two states manages to recover between 5 and 10 % more energy than a reference DC/DC-converter when running the two drive cycles used.

*Keywords: Waste heat recovery, thermoelectric generator, maximum power point tracking*

# Sammanfattning

En ökande efterfrågan på lägre bränsleförbrukning ökar kraven på totalverkningsgraden i lastbilar. Då effektiviteten hos en modern dieselmotor är ungefär 40 % produceras stora mängder spillvärme.

Återvinning av denna spillvärme kan göras med termoelektriska generatorer. Spänningen och den inre resistansen hos dessa generatorer är dock temperaturberoende, vilket resulterar i olika optimala strömmar för olika arbetsförhållanden enligt teoremet om maximal effekt.

Att ansluta generatorerna till en DC/DC-konverter med Maximum Power Point Tracking-teknik (MPPT) kan avhjälpa detta problem. Att växla mellan olika uppsättningar av serie- och parallellkopplingar kan även det lösa problemet.

I denna uppsats studeras återvinningspotentialen för flera olika anslutningsmetoder för en uppsättning med en effekt om några tiotals watt.

Det visas att växling mellan olika kopplingar kan medföra att mer energi återvinns än med en DC/DC-konverter. Mer arbete behövs dock för att avgöra vilka lösningar som lämpar sig för uppsättningar med effekter om flera kW.

Resultaten visar att ett switchnätverk som kan växla mellan två tillstånd återvinner mellan 5 och 10 % mer energi än en referenskonverter när de två använda kör cyklerna körs.

# Contents

<b>Abstract</b>	<b>I</b>
<b>Sammanfattning</b>	<b>II</b>
<b>Nomenclature</b>	<b>VI</b>
<b>Abbreviations</b>	<b>VII</b>
<b>1 Introduction</b>	<b>1</b>
1.1 Project background . . . . .	1
1.2 Degree project goals . . . . .	2
1.3 Limitations . . . . .	2
<b>2 The thermoelectric generator</b>	<b>3</b>
2.1 The physics of a TEG . . . . .	3
2.2 Construction of thermoelectric modules . . . . .	4
2.3 TEG performance . . . . .	4
2.4 Maximum power theorem . . . . .	5
2.5 Traditional TEG applications . . . . .	6
<b>3 Implementation possibilities for TEGs in trucks</b>	<b>8</b>
3.1 Waste heat from combustion engines . . . . .	8
3.2 The electrical system . . . . .	9
<b>4 Direct connection with and without Serial/Parallel-switching</b>	<b>10</b>
4.1 Direct connection . . . . .	10
4.1.1 Serial/Parallel switching . . . . .	10
4.2 Deciding Serial or parallel connection . . . . .	12
<b>5 DC/DC-converter connection</b>	<b>14</b>
5.1 The Buck-converter . . . . .	14
5.2 The Boost-converter . . . . .	15
5.3 The Buck/Boost-converter . . . . .	16
5.4 The Ćuk-converter . . . . .	16
5.5 The SEPIC-converter . . . . .	17
5.6 DC/DC-conversion transfer functions . . . . .	17
5.7 Converter comparison . . . . .	17
5.8 MPPT algorithms for DC/DC-converters . . . . .	18

<b>6</b>	<b>Simulink model development</b>	<b>19</b>
6.1	Model development . . . . .	19
6.1.1	TEG model and test rig . . . . .	19
6.1.2	DC/DC-converter models . . . . .	20
6.1.3	Direct connection model . . . . .	21
6.1.4	Battery & load models . . . . .	21
6.1.5	Temperature source block . . . . .	21
6.1.6	MPPT-algorithm . . . . .	22
6.1.7	Component dimensions . . . . .	23
6.2	Simplifying the switched models . . . . .	25
6.3	Complete model overview . . . . .	26
6.3.1	Short time simulations for MPPT-verification . . . . .	26
6.3.2	Efficiency maps . . . . .	26
6.3.3	Actual drive cycle . . . . .	26
6.4	Model limitations and simplifications . . . . .	26
6.5	The impact of the simplifications . . . . .	27
<b>7</b>	<b>Simulation scenarios</b>	<b>29</b>
7.1	Short time simulations for MPPT-verification . . . . .	29
7.2	Efficiency maps . . . . .	29
7.3	Actual drive cycles . . . . .	30
<b>8</b>	<b>Simulation results &amp; Conclusions</b>	<b>31</b>
8.1	Short time simulations for MPPT-verification . . . . .	31
8.2	Efficiency maps . . . . .	32
8.3	Actual drive cycle . . . . .	32
8.4	Conclusions . . . . .	33
<b>9</b>	<b>Discussion &amp; Further work</b>	<b>35</b>
	<b>Bibliography</b>	<b>37</b>
	<b>Appendices</b>	<b>39</b>
<b>A</b>	<b>TEG test rig</b>	<b>39</b>
<b>B</b>	<b>Component values</b>	<b>40</b>
B.1	For all converters . . . . .	40
B.2	Boost . . . . .	40
B.3	Ćuk . . . . .	40
B.4	SEPIC . . . . .	40
<b>C</b>	<b>MPPT-algorithm code</b>	<b>41</b>
<b>D</b>	<b>Model overviews</b>	<b>42</b>
<b>E</b>	<b>Efficiency maps DC/DC</b>	<b>44</b>
<b>F</b>	<b>Efficiency maps Serial/Parallel</b>	<b>47</b>
<b>G</b>	<b>Drive cycle results</b>	<b>49</b>



# Nomenclature

$\alpha$	Seebeck coefficient	$V \cdot K^{-1}$
$\eta$	Recovery efficiency	–
$\eta_{cycle}$	Cycle recovery efficiency	–
$\kappa$	Thermal conductivity	$W \cdot m^{-1} \cdot K^{-1}$
$\rho$	Electrical resistivity	$\Omega \cdot m$
$D$	Duty cycle	–
$\Delta D$	Duty cycle step size	–
$E$	Recovered energy	$kWh$
$E_{max}$	Maximum recovered energy	$kWh$
$f_D$	Duty cycle update frequency	$Hz$
$f_s$	Switching frequency	$Hz$
$I$	Current	$A$
$I_l$	Load current	$A$
$I_L$	Inductor current	$A$
$\Delta I$	Current ripple	$A$
$M$	Number of parallel TEGs	–
$N$	Number of serial TEGs	–
$P_{in}$	Input power	$W$
$P_{int}$	Internal power	$W$
$P_l$	Load power	$W$
$P_{max}$	Maximum Power	$W$
$P_o$	Output power	$W$
$P_s$	Switching power	$W$
$R_{batt}$	Battery resistance	$\Omega$
$R_l$	Load resistance	$\Omega$
$R_{int}$	Internal resistance	$\Omega$
$S$	Seebeck coefficient (See $\alpha$ )	$V \cdot K^{-1}$
$t_D$	Duty cycle update period time	$s$
$t_{off}$	On-state time	$s$
$t_{on}$	On-state time	$s$
$t_{on,off}$	Transistor turn on and off time	$s$
$t_p$	Switching period time	$s$
$T$	Absolute temperature	$^{\circ}C$
$T_{avg}$	Average temperature	$^{\circ}C$
$T_C$	Cold side temperature	$^{\circ}C$
$T_H$	Hot side temperature	$^{\circ}C$
$\Delta T$	Temperature difference	$K$
$u_{batt}$	Battery voltage	$V$
$u_{in}$	Input voltage	$V$
$u_o$	Output voltage	$V$
$u_{ol}$	TEG open load voltage	$V$

# Abbreviations

DC	Direct current
EGR	Exhaust gas recirculation
MOSFET	Metal oxide semiconductor field-effect transistor
MPPT	Maximum power point tracking
P&O	Perturb and Observe
PWM	Pulse width modulation
RPM	Revolutions per minute
Ser/Par	Serial/Parallel
SEPIC	Single ended primary inductor converter
TEG	Thermoelectric generator
TEM	Thermoelectric module
WHR	Waste heat recovery

# Chapter 1

## Introduction

### 1.1 Project background

The energy situation has changed radically over the last 50 years, both locally in Sweden and globally. One of the most obvious trends is the rising price of oil-based fuel, but also the prices of other energy sources are rising.

This, combined with the increasing interest for environmental effects has created a demand for services and products with higher efficiency and smaller environmental footprint in a wide array of businesses. This also applies to the transportation industry and vehicle manufacturers. One example is the introduction of hybrid and electric cars.

The energy usage needed for a certain service or product can in general be reduced in three ways:

1. Decrease the demand of the service or product
2. Exchange the energy source
3. Perform the service in a more efficient way

Electric vehicles are an example of the second way and hybrid vehicles of the third way.

It is considered to be hard to replace the oil based fuels and turn the production into alternative engine types. [1] Also, in Sweden, oil-based energy sources dominate the transportation sector with gasoline and diesel providing 87 % of the energy used in the sector year 2010, this is a decrease of only 1 % since 2009. [2] These facts rule out the second option.

The demand for goods transportations is dependant of other activities in the society, which caused a decrease in truck transports in 2009. However, the kilometres driven by swedish trucks domestically have increased from 2000 to 2011, telling us that the demand for truck transports seem to increase, rather than decrease. [3]

With this in mind, it becomes very interesting to increase the overall efficiency for the trucks in charge of the truck transports. To reuse the waste heat is one way to do this, hence the fuel consumption can be reduced. To realise this, the use of thermoelectric generators (TEGs) is an interesting possibility. Connected to the direct current (DC) system of a truck, they can provide power to the loads and charge the battery.

## 1.2 Degree project goals

- Make a study of the possibilities to connect TEGs directly to the DC-system, using serial/parallel switching.
- Make a study of common DC/DC-converter topologies and determine which topologies are suitable for the given conditions.
- Develop models and simulate the possible and relevant solutions using Simulink and determine the best solution for connecting the TEG. The simulations should be representative for real applications, preferably originating from actual drive cycles.
- The main objective for the project is to determine whether a Serial/Parallel-switching network is a realistic option to a DC/DC-converter.

## 1.3 Limitations

Since the time for the Degree project is limited, focus is firstly put on modelling the interface between the thermoelectric generator and the load, and less time on the thermoelectric generator and the load. Also, the models for the interface needs to be kept reasonably simple, as this is just a first step in determining whether a switching network or a DC/DC-converter should be used.

In the project, focus will be on a rig of thermoelectric generators with a power output in the range of tens of watts. The aim of the project is to determine how these should be connected to regenerate as much energy as possible during complete drive cycles, not to create numbers for how much energy a waste heat recovery (WHR) system of several kW can save, and how that affects the economy of the truck.

Also, focus is put on how to maximise the energy transfer to the load, not considering that a battery e.g. can be over-charged.

## Chapter 2

# The thermoelectric generator

Thermoelectric effects have been known for a long time. 1821 Tomas Johann Seebeck discovered the phenomena that would later be named after him, without understanding what he actually saw. Later, Jean-Charles Peltier discovered the reversed effect in 1834. Even if the effects have been long known, practical applications were limited. Only lately the interest of using thermoelectric effects to recover waste heat has risen.

### 2.1 The physics of a TEG

A TEG gives the possibility to directly convert thermal energy to electric energy. This possibility is derived from the fact that charge carriers in conducting materials are affected by heat flows in the conductor, namely that they move with the flow. Thus, a heat flow can induce a current in a conductor and vice versa. In metals, the current is carried by the shared electrons in the metallic material. In semiconducting n- and p-doped materials, the injected electrons and holes carry the current respectively.

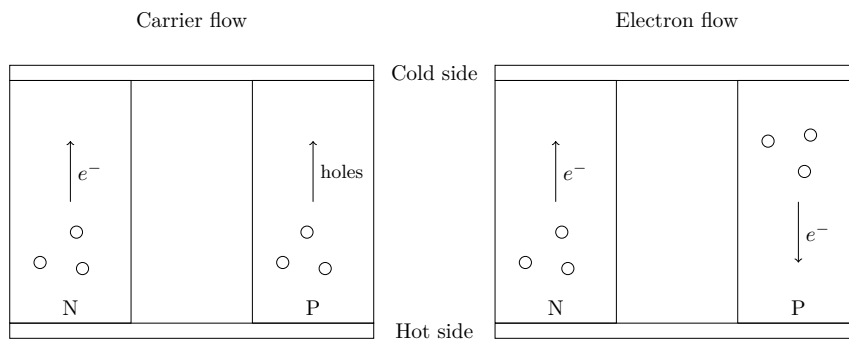


Figure 2.1: Charge carrier and electron flow in p and n materials

For a regular metal conductor, a heat flow would cause the charge carrying

electrons to move in the same direction as the heat energy flows. However, in a p-doped semi conductor, a heat flow in a certain direction would cause the holes to flow in the same direction, essentially causing electrons to move in the opposite direction. Figure 2.1 illustrates how the charge carriers and electrons are affected when a closed circuit consisting of a thermocouple of one p- and one n-doped leg is exposed to a temperature difference.

Different materials are affected differently by heat flows. One factor describing the thermoelectric characteristics of a material is the Seebeck coefficient. Study the piece of a homogenous conducting material with different temperatures at the two ends in Figure 2.2. If the material is a thermoelectric material, a voltage of  $u = \alpha(T_1 - T_2)$  is developed between the ends of the piece.

$$\alpha = V/\Delta T \quad (2.1)$$

Equation 2.1 defines the Seebeck coefficient.  $S$  can also be used instead of  $\alpha$ , and sometimes it is referred to as thermal emf or thermopower. [4]

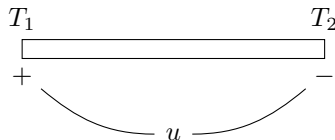


Figure 2.2: Defining  $\alpha$

Since the Seebeck coefficient has a low magnitude, it is often more convenient to write it as  $\mu V/K$  than  $V/K$ .

## 2.2 Construction of thermoelectric modules

The fact that a heat flow in one direction causes one p- and one n-doped material to induce electron currents in different directions, raises the possibility to connect several blocks of materials electrically in series, but thermally in parallel. This means that the induced currents will be working in the same direction and not cancel each other. Connecting several blocks in series can raise the output voltage to useable levels in comparison to the few  $mV$  generated by a single block. The construction principle can be seen in Figure 2.3, where three thermocouples are used. In commercial thermoelectric generators, several couples are used, ranging from tens to hundreds. [5]

## 2.3 TEG performance

In both industries and research, the unitless *figure-of-merit*, or  $ZT$ , has been commonly accepted as a measurement of TEG performance.  $ZT$  is defined as

$$ZT = \frac{\alpha^2 T}{\rho \kappa} \quad (2.2)$$

where  $\rho$  is the electric resistivity,  $\kappa$  the thermal conductivity and  $\alpha$  the Seebeck coefficient.  $ZT$  is derived by studying the conversion efficiency for a

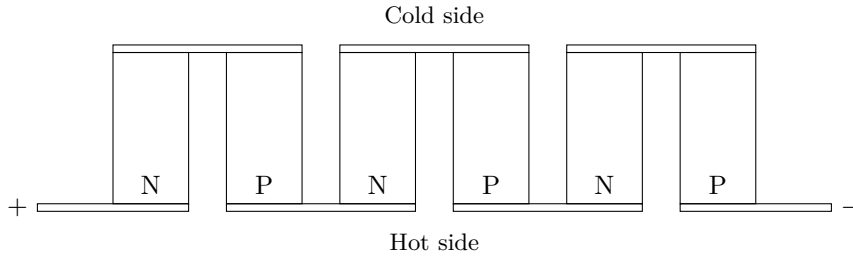


Figure 2.3: Principal construction of a Thermoelectric module

power generating TEG as in [6], and it indicates approximately which efficiencies that can be expected from a TEG given its material parameters. Note that  $ZT$  is temperature dependent and that the TEG performance is strongly dependent of the working conditions. Materials that posses a  $ZT$  higher than 0.5 are usually considered thermoelectric materials. [7]

## 2.4 Maximum power theorem

In order to be able to simulate and predict how a TEG will behave in an electric circuit, a model must be created. Therefore, the TEG will be looked upon as its Thévenin equivalent circuit.

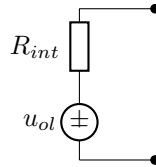


Figure 2.4: Thévenin equivalent circuit for TEG

The open load voltage  $u_{ol}$  and the internal resistance  $R_{int}$  will be material and temperature dependent parameters. When connecting a load resistance,  $R_l$  to the equivalent circuit, an expression for the power transferred to the load can be derived.

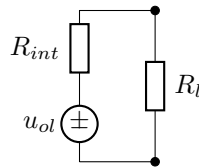


Figure 2.5: Thévenin equivalent circuit for TEG with a resistive load connected

The current flowing through  $R_l$  will be equal to

$$I_{R_l} = \frac{u_{ol}}{R_{int} + R_l} \quad (2.3)$$

and the load power will be equal to

$$P_l = R_l I_{R_l}^2 = \frac{u_{ol}^2 R_l}{(R_{int} + R_l)^2} \quad (2.4)$$

This power equation is maximised when

$$R_l = R_{int} \quad (2.5)$$

To illustrate how the load resistance affects the power transferred to the load, figure 2.6 shows a MATLAB plot of the powers  $P_l$  and  $P_{int}$  as a function of the load resistance  $R_l$  when  $u_{ol} = 10\text{ V}$  and  $R_{int} = 5\ \Omega$ .

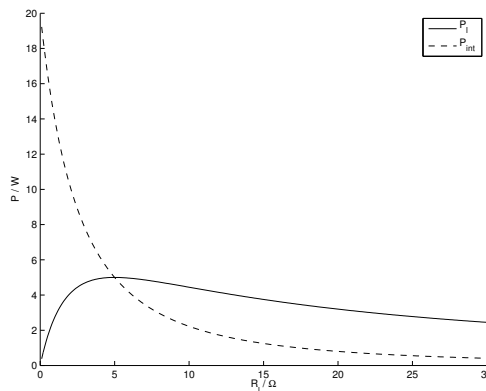


Figure 2.6: Power plot of TEG equivalent circuit with varying load resistance

Note that in the optimal case, only half of the power is transferred to the load and the other half is wasted in the internal resistance. This ratio can be improved by increasing the load resistance, however, both the load power and internal resistance power will decrease by doing this.

To verify this theory, measurements was made on an experimental rig<sup>1</sup>. The output power of the rig is plotted as a function of the current. The plot in Figure 2.7 confirms that there definitely is a point where the output power is maximised, and that other operating points result in less power.<sup>2</sup>

## 2.5 Traditional TEG applications

Because of the low efficiency and high investment costs, the use of TEG for energy harvesting has been limited. Instead, the component has been used for temperature measurements in most cases, heat pumping in some cases and energy harvesting only in rare cases. The TEG has been used in space applications, *Voyager 1*, that left Earth in 1977, was powered by a 159 W TEG heated by radioactive isotopes [8]. Several spacecrafts has been powered by thermoelectric generators, including several of the *Apollo* and *Pioneer* crafts. Generators

<sup>1</sup>For further information about the test rig, see section 6.1.1 and Appendix A

<sup>2</sup>The reason for the scattered values that is not following an ideal curve shape is limitations in the measurement process, further explained in Appendix A

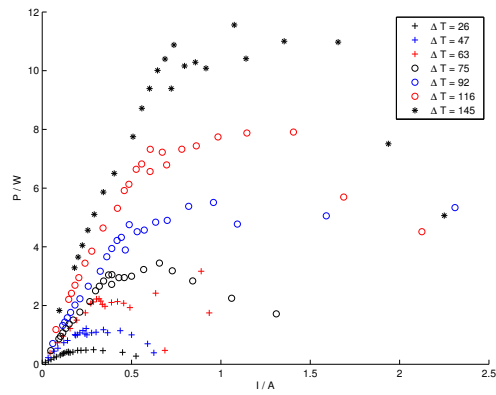


Figure 2.7: Power plot of test rig for different  $\Delta T$ s

powered by nuclear heat has been proven a reliable and long-lived power source. [9]

Both Seiko and Citizen have built wrist watches powered by thermoelectric generators. The Seiko watch generator could produce  $22 \mu W$  electric power under normal conditions. [10]

## Chapter 3

# Implementation possibilities for TEGs in trucks

### 3.1 Waste heat from combustion engines

Combustion engines suffer from low efficiency. Traditionally this hasn't been a problem neither economically or environmentally<sup>1</sup>, it has only been a matter of transporting the large amounts of waste heat away from the vehicle. However, the waste heat can be seen as a "free" source of energy.

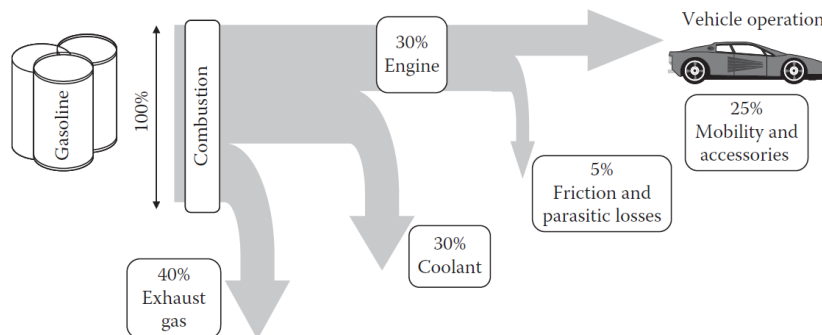


Figure 3.1: Typical energy flow in a vehicle [11]

As can be seen in Figure 3.1, the energy losses are distributed in several ways. In this project, focus is put on a small part of the exhaust gas energy, namely the exhaust gas recirculation-gases (EGR-gases).

In modern diesel engines, small amounts of exhaust gas can be recirculated to the engine air intake in order to precisely control the combustion temperature. This is done to decrease the amount of nitrogen oxides generated. These gases typically holds a high temperature since they are separated from the exhaust gases before the catalytic converter, and they typically have to be cooled in

<sup>1</sup>More precisely, the environmental problem was yet to be identified.

order to control the combustion temperature effectively. Note, however, that the EGR-gas flow is low compared to the exhaust flow, possibly limiting the amount of available energy. [12, 13]

Waste heat recovery systems can in theory be installed wherever waste heat is present, in this project, focus will be put on the EGR-gases.

## 3.2 The electrical system

Among the conventional trucks being mass produced today, a 24 V system is the most common solution.

Hybrid trucks will however need to have a high voltage system driving the electric machine. The reason for this is the high currents required to deliver a high power with a low voltage. With high currents follow high resistive losses and large cross section surface areas for the conductors. Using a higher voltage can solve these problems, but also introduce new problems.

For example, a higher voltage can introduce safety issues. One is that rescue personal working with damaged vehicles may be exposed to the high voltage. Also, the battery pack needs to provide a higher voltage than before. The batteries can either provide a high enough voltage themselves for the electric machine, or, a slightly lower voltage level can be boosted to be useable. To provide such a high voltage, several battery cells have to be serially connected.

Alongside with the high voltage system, a traditional 24 V system may exist to power the traditional electric loads. This brings forth questions whether there should exist both high voltage and low voltage batteries in a single truck, and if power transfer between the systems should be non-existent, one directional or two directional.

This also raises the question whether the TEGs should be connected to a 24 V system or a system of around 500 - 750 V.

One philosophy regarding this is to compare the power of the WHR system, the auxiliary loads and the traction motor. If the power of the WHR system is less than the typical auxiliary load, the WHR system can be connected to the 24 V system. If the power on the other hand overshoots the auxiliary load power, the WHR system can be connected to the high voltage system. [14]

In Figure 3.2, a generic block diagram of an electrical system can be seen. This picture will be extended when discussing different connections of the TEGs.

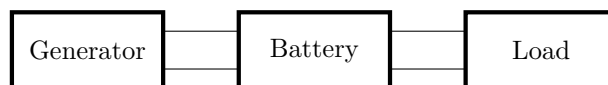


Figure 3.2: Block diagram of a generic electrical system

## Chapter 4

# Direct connection with and without Serial/Parallel-switching

### 4.1 Direct connection

Thermoelectric generators can be more or less be connected directly to a load or battery. When connecting to a battery, the TEG will need to produce a higher output voltage than the battery voltage, otherwise the TEG will be working as a Peltier heat pump<sup>1</sup>. To prevent this, a diode is added between the battery and TEG.

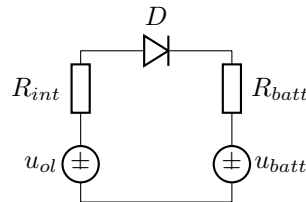


Figure 4.1: TEG directly connected to a battery

A problem with this connection technique is that the temperature dependencies of  $u_{ol}$  and  $R_{int}$  combined with a varying load resistance will cause the operating point of the TEG to vary. This can create a situation where only a fraction of the potential energy is actually recovered. Figure 4.2 shows how a directly connected TEG-rig fits into the block diagram of the electrical system.

#### 4.1.1 Serial/Parallel switching

A possible solution, or damage control, of this problem is to change the number of series and parallel connected generators, changing the open load voltage and

<sup>1</sup>The very same component as the TEG, but used differently. A Peltier uses electric energy to transport heat, a TEG uses thermal energy to generate electric energy.

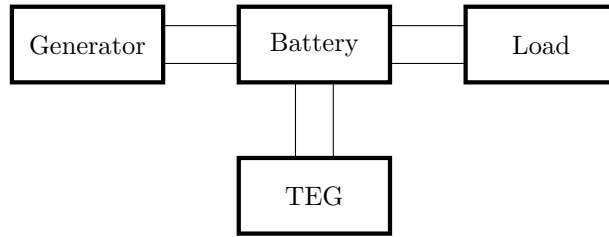


Figure 4.2: Block diagram of a generic electrical system with a directly connected TEG-rig

internal resistance, to maximise the output power. The possibility of switching ways the generators are connected during operation could be a possible way to increase the efficiency.

Assuming that one TEG has an open load voltage of  $u_{ol}$  [V] and the internal resistance  $R_{int}$  [ $\Omega$ ], expressions for the open load voltage and internal resistance for an array of generators, with  $N$  serially connected and  $M$  parallel connected, can be derived as:

$$\begin{cases} u_{ol,array} = u_{ol} * N \\ R_{int,array} = R_{int} * \frac{N}{M} \end{cases} \quad (4.1)$$

Such an array can be seen in figure 4.3.

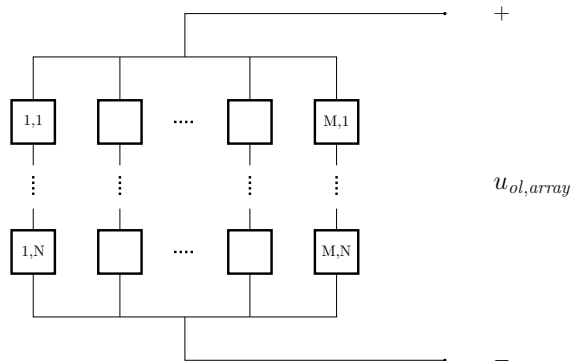


Figure 4.3:  $M * N$  size TEG array

Figure 4.4 shows the relative power output of two serial connected and two parallel connected generators connected to a load  $R_l$ . As can be seen, both reach the maximum theoretical power, but at different load resistances, or different output currents.

In this project, two different switching networks will be simulated. The switches can be realised by either electromechanical relays or transistors. The first layout allows two TEG-blocks to be connected either in series or parallel. The other layout allows four TEG-blocks to be connected either all in series, two in series and two in parallel and lastly all in parallel.<sup>2</sup> The networks can be seen in Figure 4.5 and 4.6.

<sup>2</sup>In theory, a lot more states are possible, but only the symmetric layouts are studied.

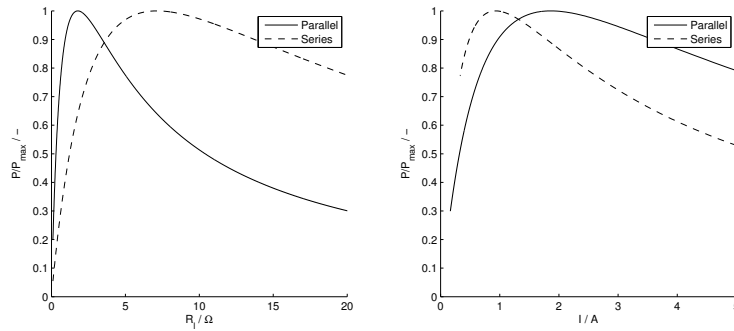


Figure 4.4: Relative power plots for serial/parallel connection

How a Serial/Parallel-switching network fits into the block diagram can be seen in Figure 4.7.

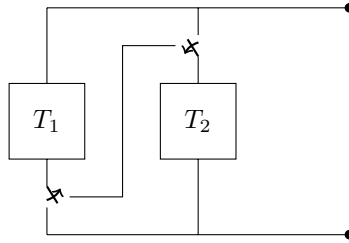


Figure 4.5: Ser/Par switching network for two blocks

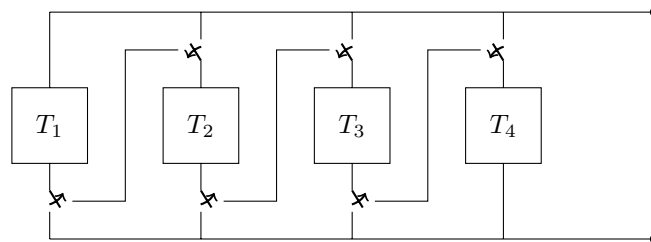


Figure 4.6: Ser/Par switching network for four blocks

## 4.2 Deciding Serial or parallel connection

Both for direct connection and DC/DC-converter connection, the question how to connect the TEGs rise. The upside of connecting the TEGs in series is that the voltage stacks, a crucial feature when using direct connection. However, if a single TEG in a series break, the whole branch becomes useless until the malfunctioning TEG is replaced or bypassed. If a failure causes a short circuit, other TEGs can be affected with a lower efficiency as a result.

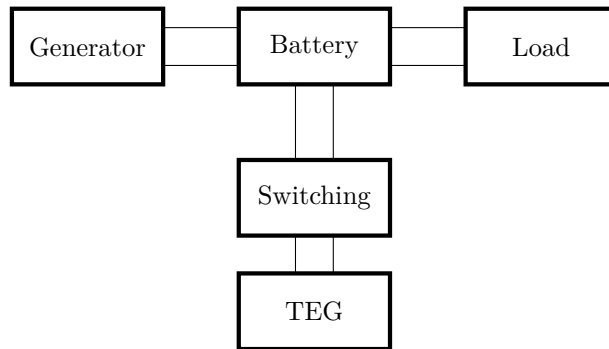


Figure 4.7: Block diagram of a generic electrical system with a Serial/Parallel-switching TEG-rig

When parallel connecting the voltage will not stack, but the currents will, allowing a higher power output. When connected in parallel, the other TEGs will not be affected if one fails, providing extra reliability.

To decide how  $M$  and  $N$  should be chosen, the following strategy is suggested:

- Select  $N$  so that the desired output voltage for typical  $T_H$  and  $T_C$  is achieved
- Select  $M$  so that the desired maximum power output is reached

How high the desired output voltage is varies with the given conditions. If direct connection is used, the maximum power will be delivered when the open load voltage equals twice the output voltage. For example, if a 24 V battery is charged with 28.5 V, the open load voltage for the TEGs should reach 57 V when operating under typical circumstances.

When using a DC/DC-converter, the voltage does not need to be raised as much since the converter will handle the small differences between the TEG output voltage and battery voltage. If the power should be delivered to a hybrid battery of several hundred volts, two stacked converters can be used if the input voltage to the converter isn't high enough.

## Chapter 5

# DC/DC-converter connection

If the output voltage of the TEGs does not overshoot the battery voltage, it is necessary to increase the output voltage in order to be able to deliver energy to the battery. This can be done by using one or many DC/DC-converters. The main purpose of a DC/DC-converter is to convert a certain voltage level to another certain voltage level. Conventional, linear converters that rely on voltage or current division are, however, inefficient and are only capable of providing an output voltage lower than the input voltage.

In this project, focus will be on hard-switching PWM<sup>1</sup> converters. These converters utilise semiconductors used as switches working either in an *on* or *off* state. In principle, the component will either not be conducting, or conducting without a voltage drop. In these two states, no power will be lost as heat. However, there is a small voltage drop when conducting causing conduction losses. Also, when switching between the states, switching losses will occur.

PWM DC/DC-converters are mainly controlled by the *duty-cycle*  $D$ .  $D$  is defined as the ratio between the *on* time of the switch and the sum of the *on* and *off* time. [15]

$$D \equiv \frac{t_{on}}{t_{on} + t_{off}} = \frac{t_{on}}{t_p} \quad (5.1)$$

In order to identify which converter type is more suitable for the given conditions, the different converter types must be studied.

### 5.1 The Buck-converter

The Buck-converter, also called the Step-down converter, is only capable of providing an output voltage equal to or lower than the input voltage. While in *on*-state, the source voltage will increase the current in the inductor  $L_1$ . As the transistor turns *off*, the inductor current can not change instantaneously and will flow through the diode  $D$  instead. In steady state operation, where the

---

<sup>1</sup>Pulse Width Modulated

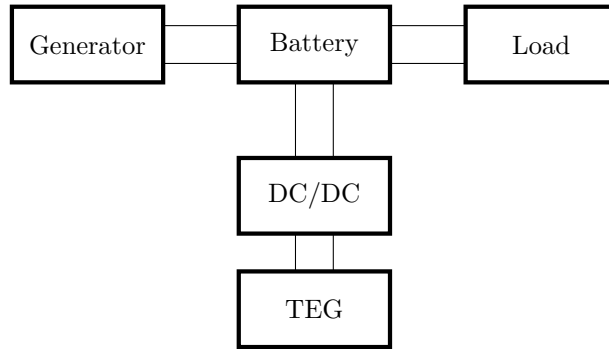


Figure 5.1: Block diagram of a generic electrical system with a TEG-rig connected through a DC/DC-converter

voltage time integral for the inductor must be zero over one period, the ratio between the input and output voltage can be derived as

$$(u_{in} - u_o)DT = -u_o(1 - D)T \quad (5.2)$$

$$\frac{u_o}{u_{in}} = D \quad (5.3)$$

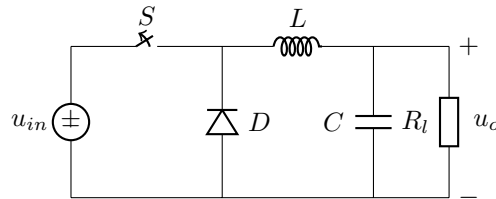


Figure 5.2: The Buck-converter

The buck converter is not capable of providing higher output voltage than the input voltage, and is therefore not interesting for our application.

## 5.2 The Boost-converter

The Boost converter is capable of increasing the input voltage, an interesting feature since this can reduce the needed number of serially connected TEGs. The ratio between the input and output voltage is derived as

$$u_{in}DT = (u_o - u_{in})(1 - D)T \quad (5.4)$$

$$\frac{u_o}{u_{in}} = \frac{1}{1 - D} \quad (5.5)$$

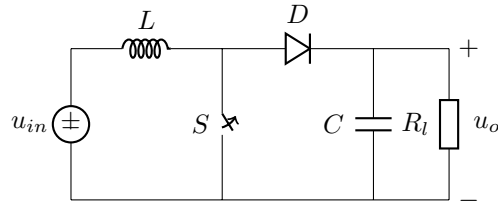


Figure 5.3: The Boost-converter

### 5.3 The Buck/Boost-converter

The third topology studied is capable of output voltages both lower and higher than the input voltage, hence the name Buck/Boost-converter.

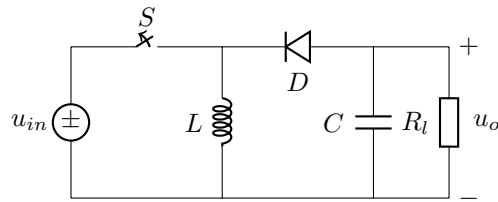


Figure 5.4: The Buck/Boost-converter

The ratio between the input and output voltages is

$$\frac{u_o}{u_{in}} = -\frac{D}{1-D} \quad (5.6)$$

[16].

### 5.4 The Ćuk-converter

Taking things a bit further, by introducing more passive components, in total two inductors and two capacitors, a Ćuk-converter can be constructed. The Ćuk-converter is capable of both increasing and decreasing the input voltage, just like the Buck/Boost-converter.

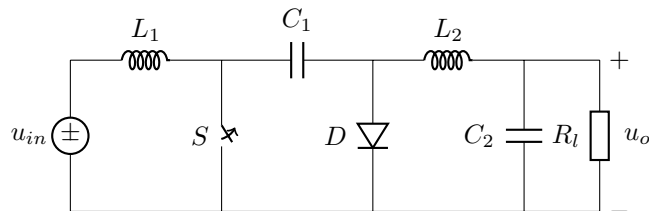


Figure 5.5: The Ćuk-converter

The transfer function for the Ćuk-converter is derived as

$$I_{L_1}(1 - D)T = I_{L_2}DT \quad (5.7)$$

assuming that the average current through the capacitor  $C_1$  is zero. For a lossless converter the input power equals the output power, thus

$$P_{in} = u_{in}I_{L_1} = -u_oI_{L_2} = P_o. \quad (5.8)$$

By combining equation 5.7 and 5.8, the voltage ratio can be written as

$$\frac{u_o}{u_{in}} = -\frac{D}{1 - D} \quad (5.9)$$

## 5.5 The SEPIC-converter

The last topology studied is called the SEPIC<sup>2</sup>-converter. The ratio between the input and output voltages is

$$\frac{u_o}{u_{in}} = \frac{D}{1 - D} \quad (5.10)$$

[17]. The SEPIC looks very similar to the Ćuk-converter, with the main difference that it is not inverting the output polarity.

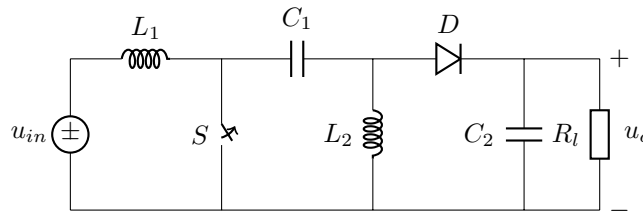


Figure 5.6: SEPIC-converter

## 5.6 DC/DC-conversion transfer functions

Table 5.1 lists the voltage transfer functions of the studied topologies.

## 5.7 Converter comparison

In this section, a comparison table of the different topologies is presented. It briefly sums up some important characteristics of the converters. The comparison deals with output polarity, where a non-inverting output allows a common ground for the TEG and battery, input current ripple, where a low ripple allows a steady operating point, drive circuit, where the grounded circuit is less complicated and finally, cost aspects, that regards the complexity of the circuit.

<sup>2</sup>Single-Ended Primary-Inductor Converter

Table 5.1: DC/DC-converter transfer functions

Converter type	Transfer function [V/V]
Buck	$D$
Boost	$\frac{1}{1-D}$
Buck/Boost	$-\frac{D}{1-D}$
Ćuk	$-\frac{D}{1-D}$
SEPIC	$\frac{D}{1-D}$

Table 5.2: DC/DC-converter comparison

	Boost	Buck/Boost	Ćuk	SEPIC
Output polarity	Non-inverting	Inverting	Inverting	Non-inverting
Input current	Non-pulsating	Pulsating	Non-pulsating	Non-pulsating
Drive circuit	Grounded	Floating	Floating	Grounded
Cost aspects	-	Floating drive circuit	Floating drive circuit & extra components	Extra components

## 5.8 MPPT algorithms for DC/DC-converters

In order to maximise the power output from the TEGs, the converters must be controlled. Control of this type is generally referred to as MPPT. The control can be done by adjusting the *duty-cycle* so that equation 2.5 is fulfilled. However, one may want to maximise the power output from the converter instead of the TEGs. This will maximise the energy transferred to the battery.

Several MPPT control algorithms exist, including *Perturb & Observe* (P&O), *Incremental conductance* and *Parasitic capacitance*. In this project, a simple P&O algorithm will be used. For further reading in this matter, [18] is recommended.

## Chapter 6

# Simulink model development

### 6.1 Model development

To be able to determine which converter topology is best suited for TEG waste heat recovery applications, Simulink models were developed for a TEG rig, several DC/DC-converters and a battery load. The different converter types were run through several scenarios where transferred energy, ripple currents and overall efficiency were compared.

As a starting point, some assumptions and design guidelines were set:

- The converter should handle 30  $W$
- The TEG open load voltage is 20  $V$ <sup>1</sup>
- The battery voltage is 12  $V$
- For the Boost- and Buck/Boost-converters, the inductor current ripple should be less than 0.5  $A$  at the maximum power output.
- A switching frequency of 40  $kHz$  is used

#### 6.1.1 TEG model and test rig

Measurements were performed on the test rig described in Appendix A in order to model the voltage and internal resistance characteristics. For three different  $T_C$ , the open load voltage and short circuit current was measured over the possible range for  $T_H$ . From this information the internal resistance can be derived. The open load voltage was found to be close to a linear function of  $\Delta T$ . The internal resistance was found close to a linear function of the approximated average TEG temperature.

$$u_{ol} \approx k\Delta T \tag{6.1}$$

---

<sup>1</sup>This open load voltage corresponds to a  $\Delta T$  of 150  $^{\circ}C$  with the test rig described in Section 6.1.1.

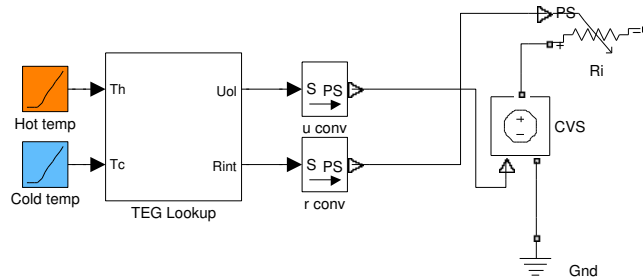


Figure 6.1: Simulink TEG model

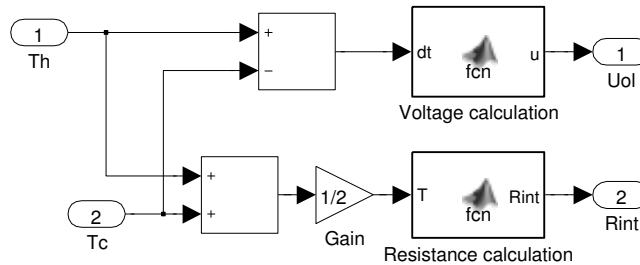


Figure 6.2: Function block for the TEG Simulink model

$$R_{int} \approx l \frac{T_H + T_C}{2} + m = l T_{avg} + m \quad (6.2)$$

For our rig, the parameter values are  $k = 0.13289 \text{ V/K}$ ,  $l = 0.032 \text{ } \Omega/\text{K}$  and  $m = 6.7 \text{ } \Omega$ . Note that these values are valid for our rig consisting of three serially connected TEGs. For one TEG, these values have to be divided by 3.

The found dependencies are supported by Equation 2.1 and the fact that the resistivity of a conductor is temperature dependant and practically linear in a wide temperature range. [19]

The TEGs are modelled as a function block in Simulink that calculates the internal resistance and open loop voltage for the input temperatures. These values control a voltage source and a resistance in Simscape that work as the input to the different DC/DC-converters. Figure 6.1 shows the TEG model with its temperature inputs, controlled voltage source and internal resistance. Figure 6.2 shows the function block where the calculations are made. More information about the test rig can be found in Appendix A.

### 6.1.2 DC/DC-converter models

All the different DC/DC-converters were modelled using *Simscape*-components. The component values that we are in control of<sup>2</sup> are calculated and chosen

<sup>2</sup>Capacitance and inductance

thereafter. The parasitic elements<sup>3</sup> are chosen as typical values for the specific components.

All DC/DC-converters modelled are controlled by a PWM-signal. This signal is generated by comparing a reference value for the duty cycle with a sawtooth wave. If the reference value is higher than the sawtooth wave, a high signal is sent to the switch, and when the reference is lower than the sawtooth wave, a low signal is sent.

### 6.1.3 Direct connection model

The direct connections are modelled as just the TEG-block, through a *Simscape*-diode, to the load.

### 6.1.4 Battery & load models

The load block is designed to represent a 12 V system, including the battery and resistive auxiliary loads. The battery model used is a modified version of the battery model included in *SimPowerSystems*. The modifications are done to make it work with *Simscape*-components.

The auxiliary load is modelled as a simple variable resistor in parallel with the battery.

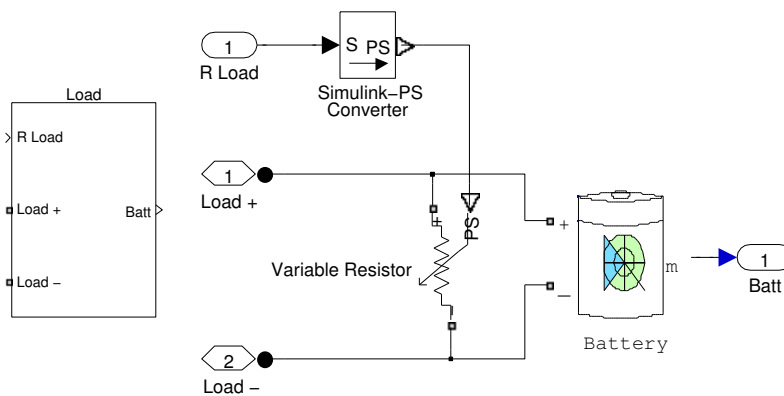


Figure 6.3: Battery & load Simulink model

### 6.1.5 Temperature source block

To be able to feed the model with realistic EGR temperature data, a block from previous works[20, 21] is implemented. This block contains torque and RPM-data from two drive cycles. This data is then ran through a look-up table where the EGR temperature is mapped as a function of the torque and RPM. This data can then be forwarded to the TEG-block when real drive cycles are being simulated.

<sup>3</sup>Series resistance and parallel conductance

### 6.1.6 MPPT-algorithm

To be able to compare the potential recovered energy from a MPPT-controlled DC/DC-converter, a simple P&O algorithm was developed. The algorithm follows and repeats a few steps:

- Measure the current output power  $P_n$
- Compare with the previous  $P_{n-1}$
- Compare current duty cycle  $D_n$  with  $D_{n-1}$
- For increasing  $P_o$ :
  - If  $D$  was increased, increase  $D$  with  $\Delta D$
  - If  $D$  was decreased, decrease  $D$  with  $\Delta D$
- For decreasing  $P_o$ :
  - If  $D$  was increased, decrease  $D$  with  $\Delta D$
  - If  $D$  was decreased, increase  $D$  with  $\Delta D$

The algorithm is executed with the frequency  $1/t_D = f_D$ . This frequency can be very low compared to the switching frequency, since the temperature and optimal operating point changes relatively slowly.

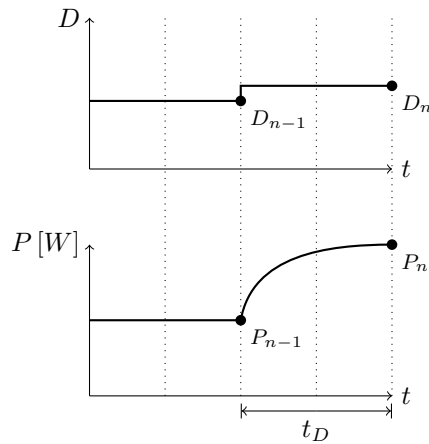


Figure 6.4: Time frame for the MPPT-algorithm

To avoid ripple disturbing the algorithm,  $P_o$  is low-pass filtered by a first order filter. The duty cycle is limited to the interval  $[0.01 \ 0.99]$ , and in order to not get stuck on the limits, code that prevents this is implemented.

The algorithm is created in an embedded *MATLAB*-code block in Simulink and the previous values of the duty cycle and output power is remembered via transport delay blocks. The code can be seen in Appendix C.

The algorithm can be improved by using a variable  $\Delta D$ , allowing the value of  $D$  to change quickly when the operating point is far from the optimal and also minimising ripple in  $D$  and  $P_o$  caused by the algorithm.

## 6.1.7 Component dimensions

### Boost-converter dimensions

Studying the *on*- and *off*-state for the converter, equations describing the current and voltage ripple in the components can be derived.

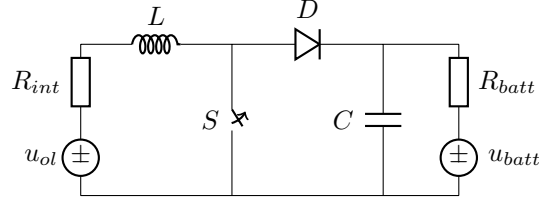


Figure 6.5: The Boost-converter with TEG and battery

When  $S$  is non conducting, the following equations will be true:

$$u_{ol} - I_L R_{int} - u_o = L \frac{di}{dt} \quad (6.3)$$

$$I_L - \frac{u_o}{R_{batt}} = C \frac{du}{dt} \quad (6.4)$$

While  $S$  is conducting, the corresponding formulas will be:

$$u_{ol} - I_L R_{int} = L \frac{di}{dt} \quad (6.5)$$

$$\frac{u_o}{R_{batt}} = C \frac{du}{dt} \quad (6.6)$$

Inserting our design parameters from Section 6.1 to equation 6.3 and 6.5 we get the following system:

$$\begin{cases} L = 10 \frac{D}{f_s di} \\ L = 2 \frac{1-D}{f_s di} \end{cases} \quad (6.7)$$

Resulting in  $D = \frac{2}{12}$  and  $L \approx 0.1 \text{ mH}$ .

### Buck/Boost-converter dimensions

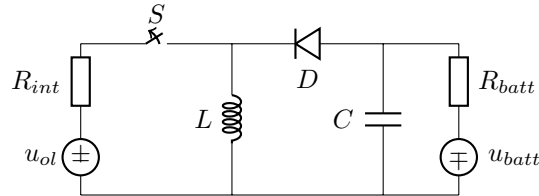


Figure 6.6: The Buck/Boost-converter with TEG and battery

The equations describing the ripples when  $S$  is non-conducting are:

$$u_o = L \frac{di}{dt} \quad (6.8)$$

$$I_L - u_o R_{batt} = C \frac{du}{dt} \quad (6.9)$$

And when  $S$  is conducting:

$$u_{ol} - I_L R_{int} = L \frac{di}{dt} \quad (6.10)$$

$$\frac{u_o}{R_{batt}} = C \frac{du}{dt} \quad (6.11)$$

Combining equation 6.8 and 6.10, the following system is achieved:

$$\begin{cases} L = 10 \frac{D}{f_s di} \\ L = 12 \frac{1-D}{f_s di} \end{cases} \quad (6.12)$$

This results in  $D = \frac{6}{11}$  and  $L \approx 0.3 \text{ mH}$ .

### Ćuk-converter dimensions

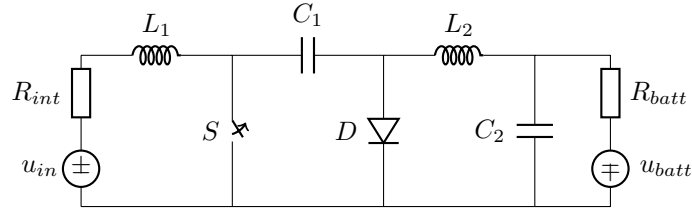


Figure 6.7: The Ćuk-converter with TEG and battery

For the Ćuk-converter, additional equations are set up for the secondary inductor. Assuming that the transfer capacitor  $C_1$  is large enough to keep a constant voltage, and that that voltage is the sum of the input and output voltage, the following equations for the two inductors are achieved:

$$\begin{cases} L_1 = 10 \frac{D}{f_s di} \\ L_1 = 12 \frac{1-D}{f_s di} \end{cases} \quad (6.13)$$

$$\begin{cases} L_2 = 10 \frac{D}{f_s di} \\ L_2 = 12 \frac{1-D}{f_s di} \end{cases} \quad (6.14)$$

These equations are identical to the ones used to dimension the Buck/Boost-converter (Equation 6.12), hence  $L_1 = L_2 \approx 0.3 \text{ mH}$ .

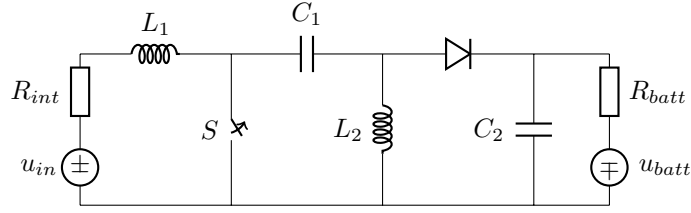


Figure 6.8: The SEPIC-converter with TEG and battery

### SEPIC dimensions

Assuming that the voltage drop across  $C_1$  is equal to the input voltage [17], the following equations are achieved:

$$\begin{cases} L_1 = 10 \frac{D}{f_s di} \\ L_1 = 12 \frac{1-D}{f_s di} \end{cases} \quad (6.15)$$

$$\begin{cases} L_2 = 10 \frac{D}{f_s di} \\ L_2 = 12 \frac{1-D}{f_s di} \end{cases} \quad (6.16)$$

These equations are identical to Equation 6.13 and 6.14, hence  $L_1 = L_2 \approx 0.3 \text{ mH}$ .

## 6.2 Simplifying the switched models

Simulating the switched converters requires a very short maximum step length for the solver. This makes it very time consuming to simulate drive cycles of several hours. In order to avoid long simulation times, some simplifications has to be made.

The strategy is to verify the functionality and behaviour of the converter model in simulations with a length less than 1 s. When simulating longer drive cycles, the theoretical maximum power will be calculated and multiplied with a steady state recovery efficiency,  $\eta^4$ , for the operating point.

The steady state efficiency is measured after letting the *MPPT*-algorithm stabilise. The hot and cold side temperatures are swept over the interesting temperature range. The efficiency can then be saved as a matrix that defines a two dimensional look-up table in *Simulink*. Focus for the cold-side temperatures will be at 10, 30 and 80 °C, and therefore these values for the cold side will be used when creating the efficiency maps.

In order to compare the switched converters to directly connected solutions, the efficiency is mapped in the same way for all different techniques. Also, the Ser/Par-switched networks are described as combinations of the efficiency maps for the direct connections that are switched between.

<sup>4</sup>Note that  $\eta$  isn't a measurement of a converters efficiency, an imagined converter could have an efficiency of 1, however, if it forces the TEG to operate in a non optimal operating point,  $\eta$  would still be low.

## 6.3 Complete model overview

In order to evaluate the functionality and energy recovery efficiency for the converters, three basic models are set up.

### 6.3.1 Short time simulations for MPPT-verification

For the short time simulations, the temperatures are fed from a signal generator to the TEG-subsystem. This subsystem controls the *Simscape*-components according to Figure 6.1. The TEG-subsystem is then connected to a converter-subsystem, containing the studied converter. Finally, this block is connected to a load-subsystem. Beyond this, extra blocks are added for measurement and plotting purposes.

### 6.3.2 Efficiency maps

The model layout for creating the efficiency maps reminds of the previous models. However, instead of generating the temperature signals with a signal builder, *MATLAB*-workspace vectors feed the temperature. Also, a block that samples the efficiency  $\eta$  is added.

### 6.3.3 Actual drive cycle

For the final simulations, only a few parts of the model is left untouched. Now the temperatures originate from two recorded drive cycles, feeding a look-up table for EGR-temperature with the torque and RPM of the engine. The gas temperature is fed to a modified TEG-subsystem, where only the maximum power output is calculated. This maximal output and the temperatures are connected to converter-subsystems where the efficiency for the current operating point is multiplied with the maximum power. The output of the converters are then fed to a subsystem where plotting and data analysis is taken care of.

## 6.4 Model limitations and simplifications

During the model development, several assumptions and simplifications has been made. In this section they are summed up and explained.

- The TEG model's voltage and resistance is assumed to be linear for any temperature. This means that very high temperatures result in very high power output, where in reality the TEG may be over its maximum temperature and break down.
- The TEG model is fed with the temperature off the EGR-gas through a low pass filter. This simulates that it will take some time for the thermal energy to reach the TEG. However, it does not consider the temperature difference that would exist in reality, where at least a pipe or a heat exchanger would be mounted between the TEG and the flowing gas.
- It is assumed that all TEGs have identical characteristics. In reality small differences can be expected.

- It is assumed that every TEG is exposed to exactly the same temperatures on the hot and cold side. In reality this would not be true.
- The model does not consider that stealing energy from the gas, the hot side of the TEG and any material in between, would lower the temperature on the hot side, and increase the temperature on the cold side.
- A switch model is used to simulate the switching transistor. While the switch has an on state resistance, it does not simulate the switching losses of a MOSFET.<sup>5</sup>
- The efficiency maps does not consider any transient behaviour of the converters, and the efficiency between the measured points is linearly interpolated.
- The efficiency maps for the Serial/Parallel-switching solutions assume that the optimal case is always used.
- The efficiency maps for the Serial/Parallel-switching solutions does not consider the ohmic losses that would occur in the switches in a real switching network.
- The look-up table for EGR-gas temperature does not cover every case in the drive cycles. Temperature data outside of the map is extrapolated.
- The MPPT-algorithm is simple, has a fixed step size and is forced to change  $D$  every step. This causes an oscillating  $D$  around the optimal  $D$ , lowering the efficiency. Close to the borders for  $D$ , a small change in  $D$  affects the transfer function heavily for some converters. A smaller step size can more precisely locate the optimal point, increasing the recovery efficiency.
- The electrical system is modelled as just a battery with a parallel load. No alternator is modelled.

## 6.5 The impact of the simplifications

The drawbacks in the TEG-model will not impact the results of the project, as the model only is used to act like a generic TEG. The same applies for the model used to generate EGR-gas temperature. Exact temperature behaviour is not needed to study the electric behaviour of the different connections.

The main issue lies in the simplifications done for the converters and Serial/-Parallel efficiency maps. In order to get an idea of how much the ohmic losses of a switching network would affect the recovery efficiency, one efficiency map was calculated with a  $0.5 \Omega$  resistor in series with the TEG-model. This is a high resistance comparing with the on-state resistance of a MOSFET and relay resistance. The difference in the efficiency maps could be seen in the second decimal, reaching up to 5 percentage points.

For the switching losses of a MOSFET, typical switching losses are calculated according to [15]. The rise and fall times are assumed to be equal and  $100 \text{ ns}$

---

<sup>5</sup>Of course, other switching components can be used and would have to be modelled according to their characteristics.

long. An open load voltage of 20 V would result in a load voltage of 10 V and 3 A at 30 W. The switching losses is then given as:

$$P_s = 2 * \frac{V_{DC} * I_0 * t_{\text{on,off}}}{2} * f_s = 10 * 3 * 100 * 10^{-9} * 40 * 10^3 = 0.12 \text{ W} \quad (6.17)$$

This power loss only makes up a fraction of the total power output, and should only affect the results to a limited extent.

# Chapter 7

## Simulation scenarios

To be able to determine the efficiency of energy recovery, some scenarios have to be set up. Some key characteristics that needs to be studied are:

- Recovery efficiency during typical steady state operation scenarios
- Tracking ability of the MPPT-algorithm through changing temperatures and loads
- Recovery efficiency throughout real drive cycles

The simulations are done in three steps, where the first simulation should verify functionality of the MPPT-algorithm, the second step should map  $\eta$  for different temperatures and the last step should show how much energy that can be recovered through two different drive cycles.

### 7.1 Short time simulations for MPPT-verification

Verification of the MPPT-algorithm is done with a one second simulation with temperature and load steps. The temperature starts at  $50\text{ }^{\circ}\text{C}$ , changes to  $100\text{ }^{\circ}\text{C}$  after  $0.25\text{ s}$  and finally changes to  $75\text{ }^{\circ}\text{C}$  after  $0.5\text{ s}$ . The load starts at  $1\ \Omega$  and changes to  $0.1\ \Omega$  after  $0.75\text{ s}$ .  $T_C$  is constant at  $10\text{ }^{\circ}\text{C}$ .

### 7.2 Efficiency maps

To decrease the simulation times, the efficiency maps described in section 6.2 needs to be created. This is done by stepping the hot side temperature in steps of  $25\text{ }^{\circ}\text{C}$  through the range from  $100\text{ }^{\circ}\text{C}$  to  $600\text{ }^{\circ}\text{C}$ . This stepping is done for the cold side as specified in Section 6.2. After each step the steady state efficiency is stored in an efficiency matrix. This matrix is then inserted into a two dimensional look up table in *Simulink*.  $10\ \Omega$  is used as a parallel load.

### 7.3 Actual drive cycles

Two real drive cycles are simulated. One is recorded in Spain and the other in the Netherlands and Belgium<sup>1</sup>. The average EGR-gas temperature for the Spain cycle is 344 °C and 277 °C for the Brussels cycle. Both cycles consist of 8 700 seconds of data.

To be able to compare the results for long, realistic drive cycles, a key number  $\eta_{cycle}$ , is defined as the quotient between the actual energy recovered during the simulation and the theoretical maximum energy that could have been delivered by the TEG if it was working in its optimum operating point during the whole cycle.

$$\eta_{cycle} \equiv \frac{E}{E_{max}} = \frac{\int_0^t P_o dt}{\int_0^t P_{max} dt} \quad (7.1)$$

This value is stored and can be used as a comparison between the different connection techniques.

Two simulations each are done for the two drive cycles, one focusing on the DC/DC-converters with 3 TEGs and one focusing on Ser/Par-switching using 8 TEGs.

---

<sup>1</sup>This drive cycle will be referred to as *Brussels*

## Chapter 8

# Simulation results & Conclusions

### 8.1 Short time simulations for MPPT-verification

Figure 8.1 shows the output power<sup>1</sup> and duty cycle of a Boost-converter. As can be seen, the algorithm quickly finds the optimal point and starts to oscillate around it. After the temperature changes, the algorithm finds the new optimal points.

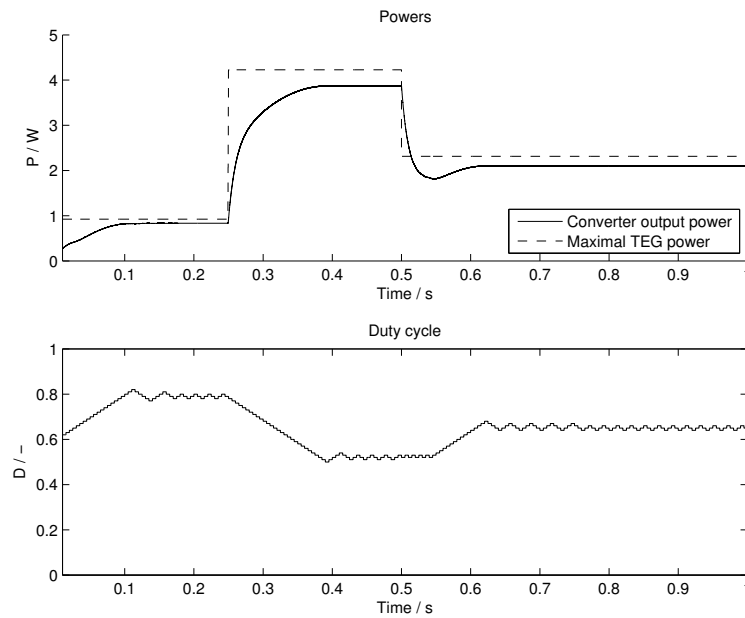


Figure 8.1: Short time simulation result

<sup>1</sup>This signal is low-pass filtered to remove the power ripple.

The load change does not seem to affect the optimal point, and passes without any change in the optimal duty cycle.<sup>2</sup>

This shows that the simple P&O-algorithm manages to track the maximum power point, even if the resolution and speed probably can be increased and the oscillation decreased.

## 8.2 Efficiency maps

The simulations provided efficiency map matrices for future use in the final model. Three dimensional plots of all efficiency maps can be seen in Appendix E and F.

## 8.3 Actual drive cycle

Table 8.1 shows the results of the simulation in form of the  $\eta_{cycle}$  for the studied DC/DC set-ups compared with the corresponding direct and serial/parallel connections.<sup>3</sup>

Table 8.1:  $\eta_{cycle}$  for the drive cycles with 3 TEGs

Connection	Spain $\eta_{cycle}$	Brussels $\eta_{cycle}$
Boost 1 * 3	0.63	0.82
Boost 3 * 1	0.83	0.81
SEPIC 1 * 3	0.85	0.88
SEPIC 3 * 1	0.77	0.78
Ćuk 1 * 3	0.85	0.88
Ćuk 3 * 1	0.77	0.77
Buck/Boost 3 * 1	0.47	0.53
Direct 1 * 3	0.64	0.83
Direct 3 * 1	0.80	0.20
Ser/Par 1 * 3 / 3 * 1	0.87	0.84

Table 8.2 shows  $\eta_{cycle}$  for the serial/parallel-connections and a reference DC/DC-converter. Appendix G shows the plotted results for the whole cycles.

It is also interesting to see to what extent the different states in the network is used. Table 8.3 contain these distributions, and Table 8.4 shows how many times the state changed during the drive cycles.<sup>4</sup>

<sup>2</sup>This could be different if there wasn't a battery connected to the load.

<sup>3</sup>Note that  $n * m$  in the connection column describes the amount and layout of the TEGs.

<sup>4</sup>The amount of state switches are valid if the switching is made ideally in order to deliver as high power as possible.

Table 8.2:  $\eta_{cycle}$  for the drive cycles with 8 TEGs

Connection	Spain $\eta_{cycle}$	Brussels $\eta_{cycle}$
1 * 8	0.30	0.43
2 * 4	0.52	0.71
4 * 2	0.80	0.87
8 * 1	0.78	0.20
2 * 4 / 4 * 2	0.81	0.91
4 * 2 / 8 * 1	0.87	0.88
1 * 8 / 2 * 4 / 4 * 2	0.82	0.92
2 * 4 / 4 * 2 / 8 * 1	0.88	0.91
SEPIC	0.78	0.83

Table 8.3: Time distribution between the states in percent

Connection	Spain	Brussels
2 * 4 / 4 * 2	32.83 / 67.17	30.99 / 69.01
4 * 2 / 8 * 1	61.58 / 38.42	99.65 / 0.35
1 * 8 / 2 * 4 / 4 * 2	23.56 / 9.27 / 67.17	7.61 / 23.38 / 69.01
2 * 4 / 4 * 2 / 8 * 1	32.83 / 28.75 / 38.42	30.99 / 68.66 / 0.35

Table 8.4: Number of state changes through the cycles

Connection	Spain	Brussels
2 * 4 / 4 * 2	92	356
4 * 2 / 8 * 1	106	6
1 * 8 / 2 * 4 / 4 * 2	176	434
2 * 4 / 4 * 2 / 8 * 1	198	362

## 8.4 Conclusions

The main purpose of this project was to investigate whether a direct connection using Ser/Par-switching could be discarded as a realistic alternative to a DC/DC-converter. The conclusion from the project is that it is; A direct connection with a switching network can definitely compete with a DC/DC-converter based solution. It may even be the better choice. However, there are practical issues that need to be taken care of.

It is shown that the converters with input inductances are far superior to converters with discontinuous input currents, such as the Buck/Boost-converter. Also, the SEPIC and Čuk-converter is working better than the Boost-converter in the simulations. However, one must consider that there is a difference in input inductor size, possibly explaining these results. The SEPIC and Čuk-converter

contains more components than a boost converter, making them more expensive and larger.

Regarding Ser/Par-switching, Table 8.3 shows some interesting things. For example, one can easily see which states are rarely used, and these states are probably not interesting to implement. However, one must also consider that only because a state is used, it does not mean that this state is working *much* better than another state. See for example the Spain cycle, when adding  $2 * 4$  as an alternative to  $4 * 2 / 8 * 1$ . The new state is used a lot, however, it does not accomplish much. This can be seen when studying how much energy is actually recovered; The gains are small. The same applies for the Brussels cycle, even though the gain in adding the state is a bit bigger. These results can be derived from the fact that the added state increases the recovery efficiency for low temperatures, where there isn't a whole lot of energy to be recovered. So, even if this energy is recovered with high efficiency, the impact on the total energy that can be recovered throughout a whole cycle is small.

Continuing with the amount of state switches seen in Table 8.4, when adding  $2 * 4$  as an option to  $4 * 2 / 8 * 1$  in the Spain cycle, the amount of state switches almost is doubled, with only small gains in recovered energy.

To sum up; One has to take great care when designing a Serial/Parallel-switching network. Adding unnecessary states results in networks that are more complex than needed and may not give better results in the end, as they will have a higher investment cost and may switch between states more often, possibly resulting in a shorter life span of the switches.

## Chapter 9

# Discussion & Further work

Since there are many simplifications in the model<sup>1</sup>, one can, and should, question the accuracy of the results. I would have liked to continue the model development further, but this would have been time consuming and out of reach within one Degree project.

However, these results should only be used as an early forecast of how the different solutions will work. With further investigations, theoretical and practical limitations and considerations may arise and change the results.

The following work is suggested to improve the models and increase the knowledge and understanding in the field:

- A model of the thermodynamic system would be necessary in order to see how much energy that could be recovered in real life. This model could for example take into account the gas flow and gas temperature where the energy will be harvested, heat exchanging to the warm side of the TEGs, thermal flow through the TEGs, cooling on the cold side, etc.
- An in-depth study of the investment cost and gains for several alternatives this could later on show which power rating and which connection type is the best from an economic perspective.
- More work will have to be put into how the TEGs interact with the rest of the system, including the battery and the alternator. The output power of the converter or TEGs can easily be maximised, but this may not always be the desired result. For example, the voltage level of the system has defined limits. The TEGs may not cause these limits to be exceeded. Also, the battery has a maximum charge level, when this is reached the battery may not absorb more energy, and the power output of the TEGs should ideally match the load power of the auxiliary loads.
- Instead of combining efficiency maps to see how Ser/Par-switching works. Several TEG-model blocks should be connected to a modelled switching network, consisting of relays or transistors. Taking into account the power that the drive-circuits will require is also recommended.

---

<sup>1</sup>Described in Section 6.4

- The DC/DC-converter models could be improved by using real transistor models instead of switches. Further, the converters design should be optimised. For example, an oversized input inductor could minimise the current ripple, resulting in a more stable operating point and higher recovery efficiency.
- Designing a smart MPPT-algorithm for the Serial/Parallel switching method. This algorithm would need to consider the economic effect of switching between states if relays are to be used. Minimising the amount of state switches without losing large amounts of energy could be the goal.
- Some drawbacks of a Serial/Parallel-switching network is mentioned in [21]. However, it must be considered if these drawbacks motivate a DC/DC-converter or if a switching network still could be the preferred alternative when considering investment costs, lifespan, energy recovery potential etc.

The effects of neglecting the switching losses and the ohmic losses of a switching network is calculated in Section 6.5. Assuming that the worst case is always the case, the better Ser/Par switching results would almost be brought down to the level of the reference DC/DC-converter. However, the operating point is not fixed and the switching network resistance is probably higher than what is realistic, reducing the losses. The switching losses are calculated to  $0.12\text{ W}$  for the TEG-rig with 3 generators. This is a very small fraction of the total power. The losses would be bigger for the 8 TEG-rig, but still the impact on the results would be very small.

# Bibliography

- [1] Chen, F.F.; *An Indispensable Truth* p. 58, Springer New York, 2011
- [2] Energimyndigheten, *Energiläget 2011* p. 73, CM Gruppen AB, 2011
- [3] Trafikanalys, *Lastbilstrafik 2011* p. 18, 2012
- [4] Rowe, D.M.; *Thermoelectrics handbook: macro to nano* pp. 1-2, CRC/Taylor & Francis, 2006
- [5] Hi-Z Technology, Inc.; *www.hi-z.com*, Product information, Gathered 2012-10-09
- [6] Rowe, D.M.; *Thermoelectrics handbook: macro to nano* pp. 1-3 - 1-6, CRC/Taylor & Francis, 2006
- [7] Rowe, D.M.; *Thermoelectrics handbook: macro to nano* pp. 1-8, CRC/Taylor & Francis, 2006
- [8] Abelson, R.D.; *Thermoelectrics handbook: macro to nano* pp. 56-1 - 56-4, CRC/Taylor & Francis, 2006
- [9] Bennet, G.L.; *CRC Handbook of Thermoelectrics* pp. 535, CRC Press, 1995
- [10] Snyder G.J.; *Energy Harvesting Technologies* pp. 326, Springer US, 2008
- [11] Stabler, F.R.; Yang, J.; *Modules, Systems and Applications in Thermoelectrics* p. 25-5, CRC Press, 2012
- [12] Binder, K.B.; Mollenhauer, K; Tschoeke, H; *Handbook of diesel engines* p. 71, Springer-Verlag, 2010
- [13] Aixala, L.; Espinosa, N.; Lazard, M.; Scherrer, H.; *Modeling a Thermoelectric Generator Applied to Diesel Automotive Heat Recovery*, Journal of Electronic materials, Vol. 39, No. 9, 2010
- [14] Professor Alaküla, M.; Interview, LTH, 120906
- [15] Alaküla, M.; Karlsson, P.; *Power Electronics: Devices, Converters, Control and Applications* p. 188, IEA, Lund University
- [16] Czarkowski, D.; *Power Electronics Handbook (Third edition)* p. 255, Butterworth-Heinemann, 2011
- [17] Gilbert, D.; Schaeffer B.; *Analysis of the SEPIC Converter*, Portland State University, 2011

- [18] Jahanbakhsh, D.; *Implementation of DC-DC converter with maximum power point tracking control for thermoelectric generator applications*, KTH Royal institute of technology, 2012
- [19] Chernoutsan, A. I.; Polyanin, A. D.; *A Concise Handbook of Mathematics, Physics and Engineering Sciences* p. 489, CRC Press, 2010
- [20] Schauman, H.; *The Thermoelectric Generator; An analysis of Seebeck-based waste heat recovery in a Scania R-series truck*, KTH Royal institute of technology, 2009
- [21] Shawwaf, A.; *Optimization of the electric properties of thermoelectric generators*, The Faculty of Engineering at Lund University, 2010

## Appendix A

### TEG test rig

A prototype rig was available during the project. The TEG-block consists of three TEGs connected in series. On both sides of every single TEG, temperature measurement blocks are placed. This allows monitoring of  $T_H$  and  $T_C$  for all three generators.

The cold side is cooled by a water cooled metal block, connected to the water system in the house.  $T_C$  can only be controlled by adjusting the water flow, not water temperature. The hot side is heated via a metal block lying on a heating element, originally designed for cooking. With this setup,  $T_H$  can reach temperatures to approximately 180 °C. The cold side can reach temperatures as low as approximately 14 °C when the heater is turned off.

These circumstances resulted in quite low precision for the measurements. However, one should remember that the goal for the project is not to create a state of the art model of these exact TEGs, these measurements were carried out to create a model that would have typical TEG characteristics.

# Appendix B

## Component values

### B.1 For all converters

Switch on state resistance	$25\text{ m}\Omega$
Switch off state conductance	$1 * 10^{-8}\ \Omega^{-1}$
Output capacitor parallel conductance	$1 * 10^{-8}\ \Omega^{-1}$
Output capacitor series resistance	$1 * 10^{-6}\ \Omega$
Output capacitor capacitance	$2.7\text{ mF}$
Diode on state resistance	$0.02\ \Omega$
Inductor series resistance	$0.2\ \Omega$
Inductor parallel conductance	$1 * 10^{-9}\ \Omega^{-1}$

### B.2 Boost

Inductor inductance	$0.1\text{ mH}$
---------------------	-----------------

### B.3 Ćuk

Primary inductor inductance	$0.3\text{ mH}$
Secondary inductor inductance	$0.3\text{ mH}$
Transfer capacitor capacitance	$2.7\text{ mF}$

### B.4 SEPIC

Primary inductor inductance	$0.3\text{ mH}$
Secondary inductor inductance	$0.3\text{ mH}$
Transfer capacitor capacitance	$2.7\text{ mF}$

## Appendix C

# MPPT-algorithm code

In the code,  $D_n$  and  $D_o$  represent the new and old values for the Duty cycle,  $P_n$  and  $P_o$  the new and old values for the output power of the converter and  $dD$  the step size of the duty cycle.

```
function D = fcn(Dn, Do, Pn, Po)

dD=0.01;

if (Dn>Do && Pn>Po)
    D=Dn+dD;
elseif (Dn>Do && Pn<Po)
    D=Dn-dD;
elseif (Dn<Do && Pn>Po)
    D=Dn-dD;
else
    D=Dn+dD;
end

if (Dn == Do && Do == 0.99)
    D = 0.97;
end

if (Dn == Do && Do == 0.01)
    D = 0.03;
end
```

# Appendix D

## Model overviews

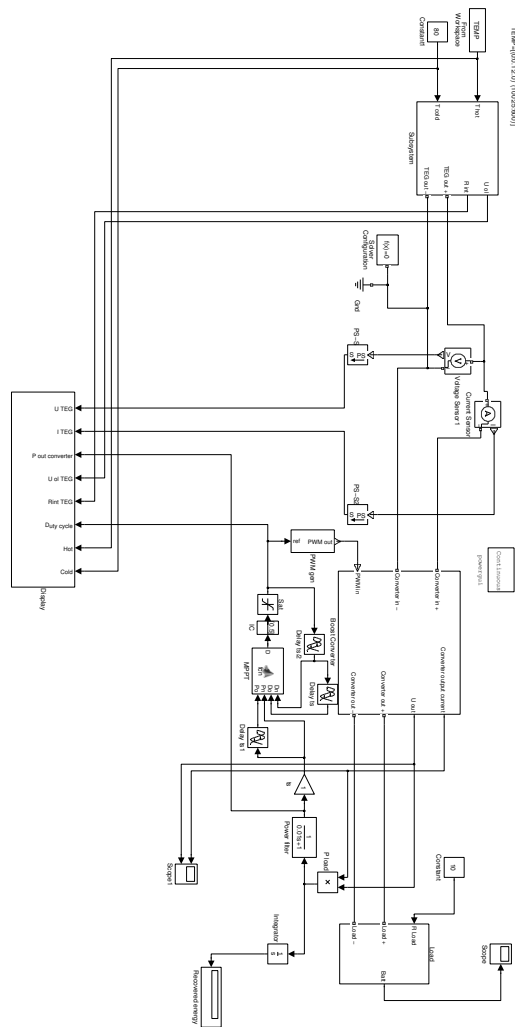


Figure D.1: Model used for efficiency mapping

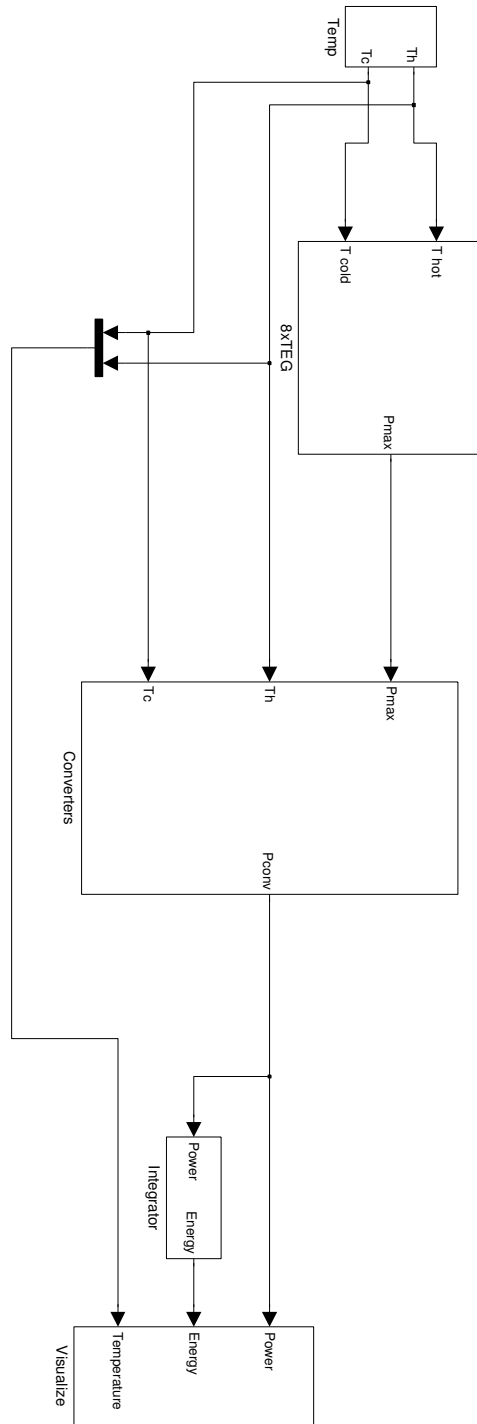
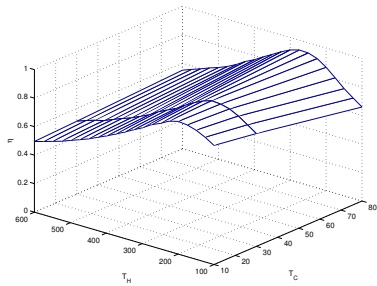


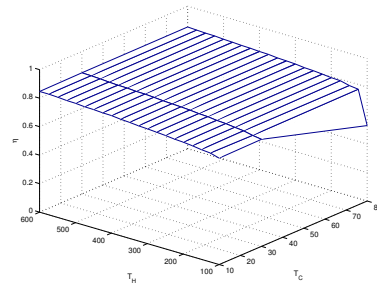
Figure D.2: Model used for real drive cycles

# Appendix E

## Efficiency maps DC/DC

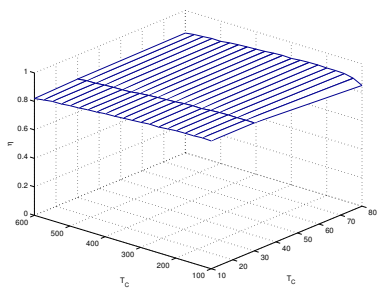


(a) 1 \* 3

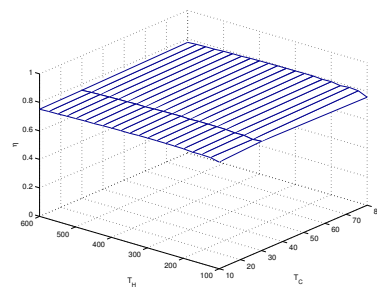


(b) 3 \* 1

Figure E.1: Boost-converter efficiency maps

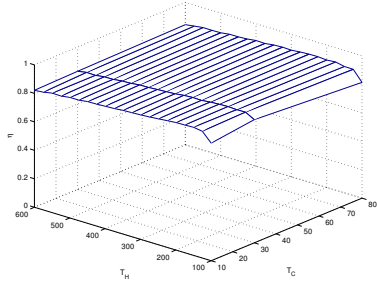


(a) 1 \* 3

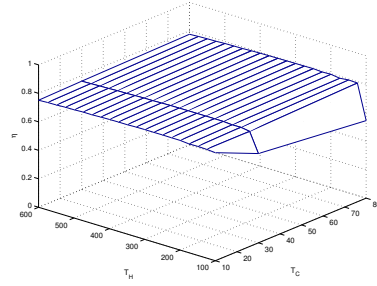


(b) 3 \* 1

Figure E.2: SEPIC efficiency maps



(a) 1 \* 3



(b) 3 \* 1

Figure E.3: Ćuk-converter efficiency maps

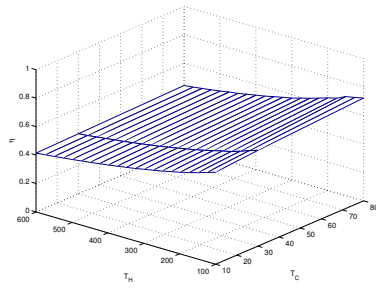
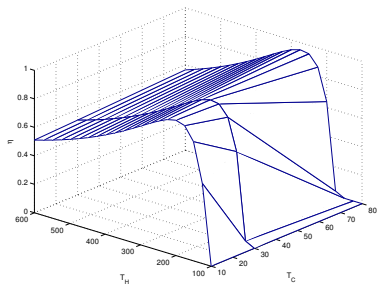
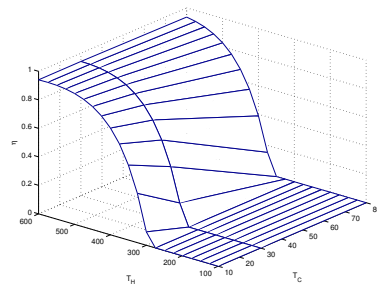


Figure E.4: Buck/Boost-converter efficiency map

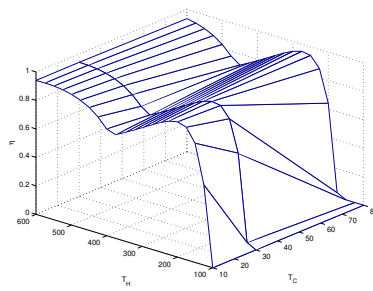


(a) 1 \* 3



(b) 3 \* 1

Figure E.5: Direct connection efficiency maps

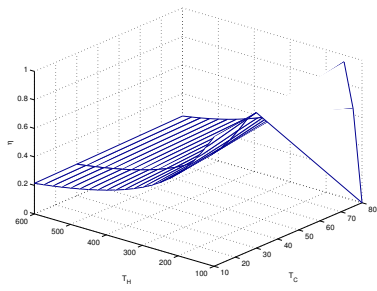


(a)  $1 * 3 / 3 * 1$

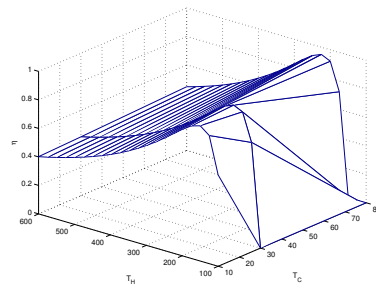
Figure E.6: Serial/Parallel switching efficiency map

## Appendix F

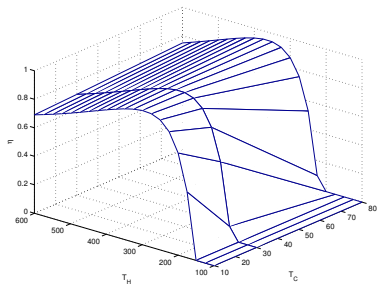
# Efficiency maps Serial/Parallel



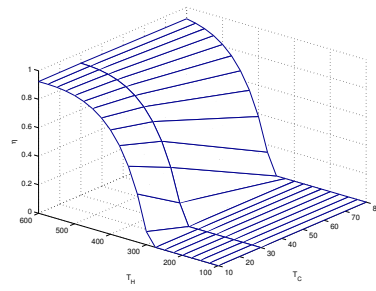
(a) 1 \* 8



(b) 2 \* 4

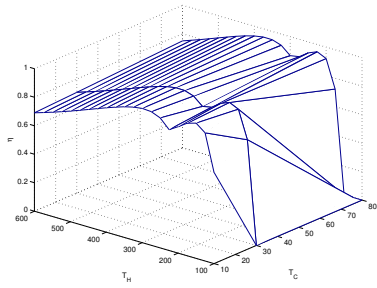


(c) 4 \* 2

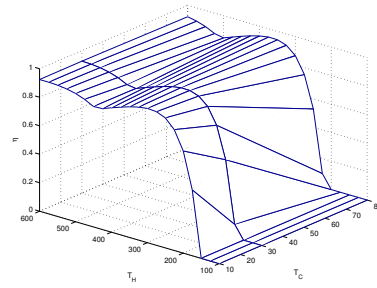


(d) 8 \* 1

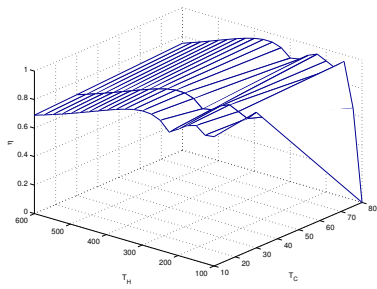
Figure F.1: Direct connection efficiency maps, 8 TEGs



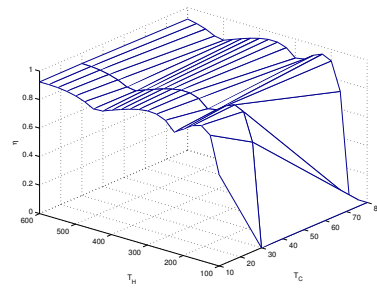
(a)  $2 * 4 / 4 * 2$



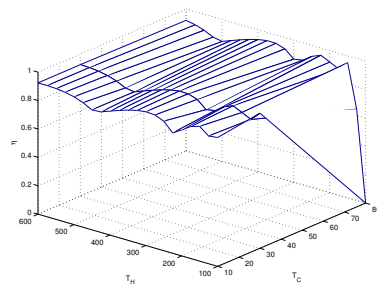
(b)  $4 * 2 / 8 * 1$



(c)  $1 * 8 / 2 * 4 / 4 * 2$



(d)  $2 * 4 / 4 * 2 / 8 * 1$



(e)  $1 * 8 / 2 * 4 / 4 * 2 / 8 * 1$

Figure F.2: Ser/Par efficiency maps, 8 TEGs

# Appendix G

## Drive cycle results

Firstly, the results for the DC/DC-converters are shown;

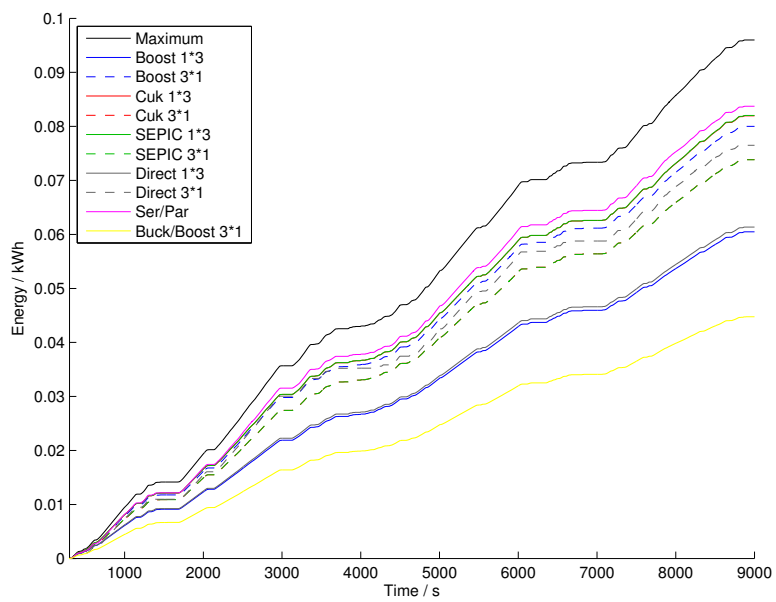


Figure G.1: Energy plot for the Spain cycle, converters

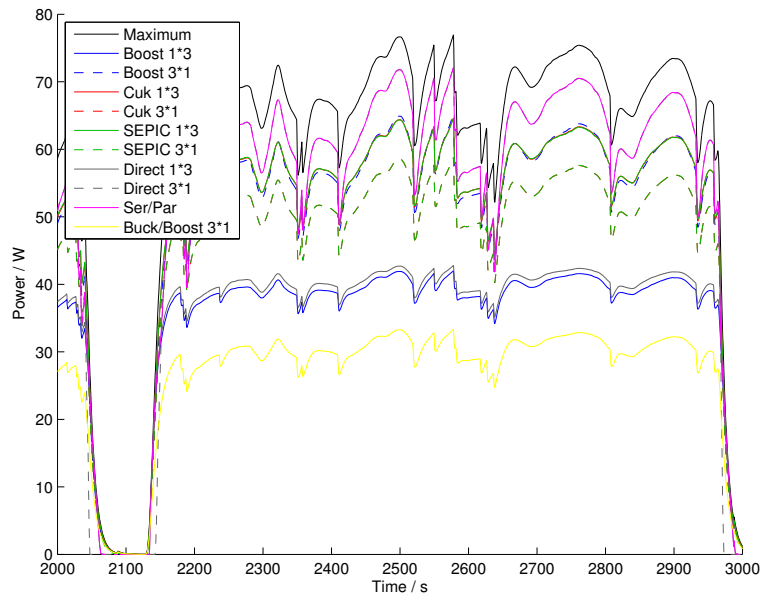


Figure G.2: Power plot for a selected time interval from the Spain cycle, converters

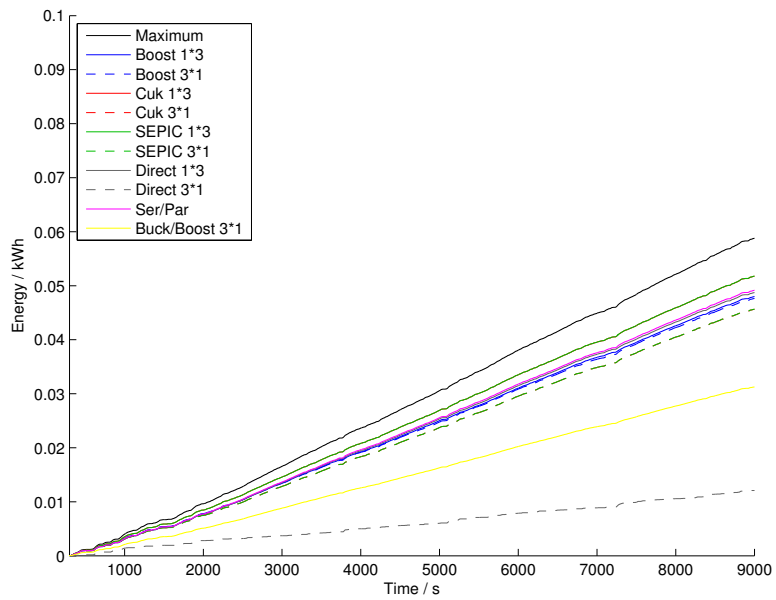


Figure G.3: Energy plot for the Brussels cycle, converters

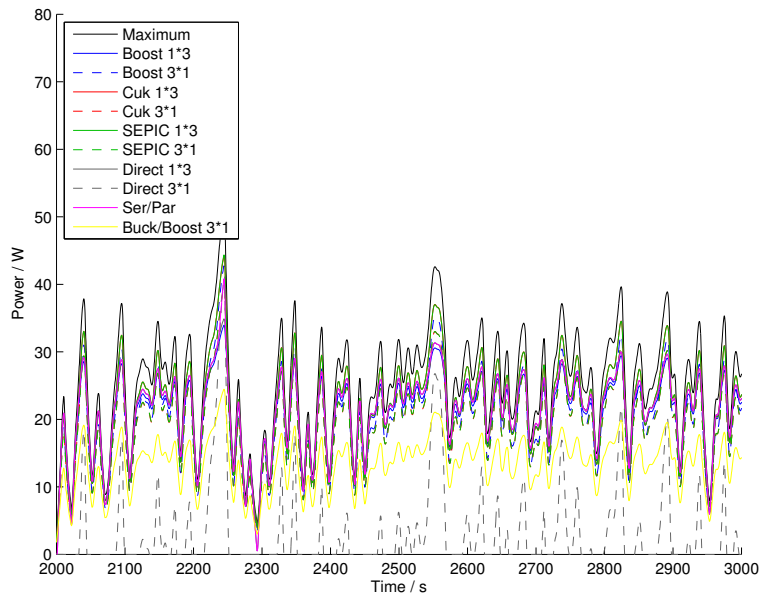


Figure G.4: Power plot for a selected time interval from the Brussels cycle, converters

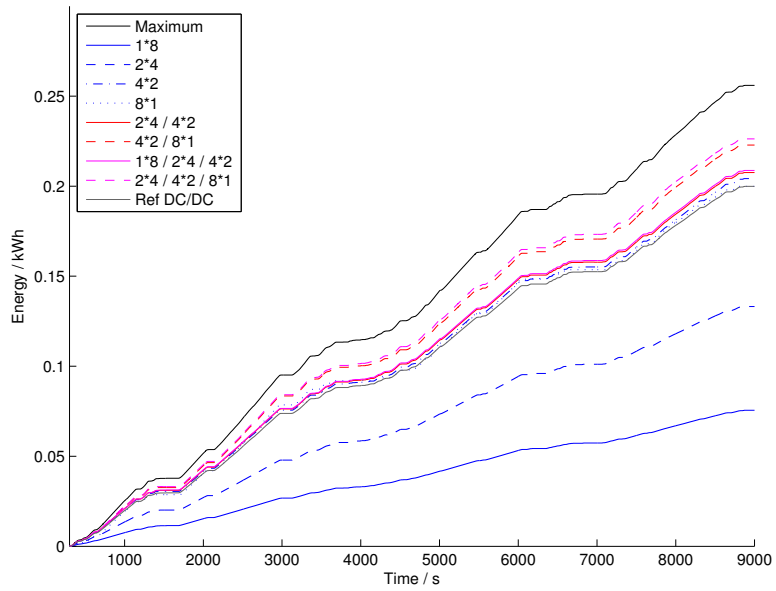


Figure G.5: Energy plot for the Spain cycle, Ser/Par

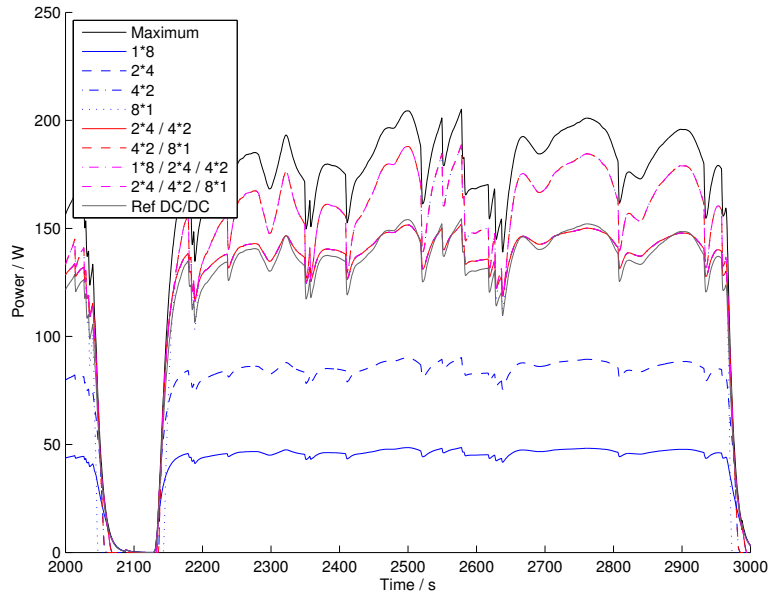


Figure G.6: Power plot for a selected time interval from the Spain cycle, Ser/Par

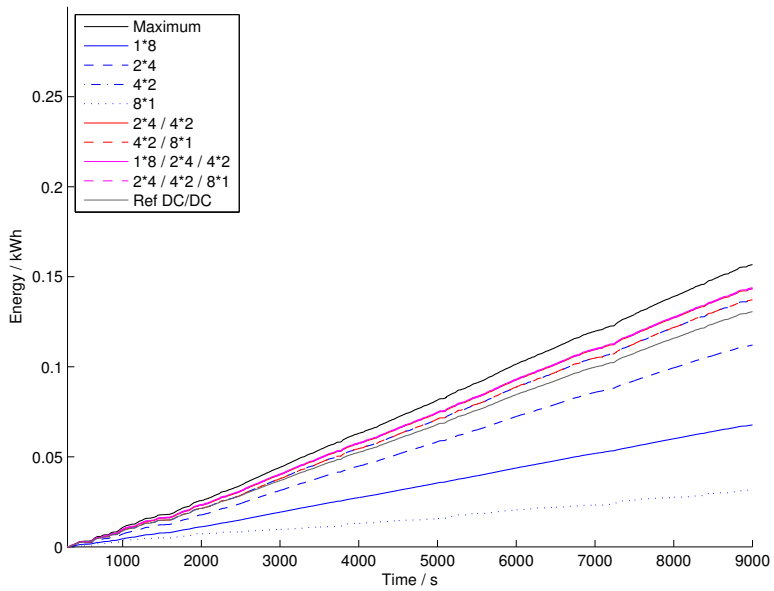


Figure G.7: Energy plot for the Brussels cycle, Ser/Par

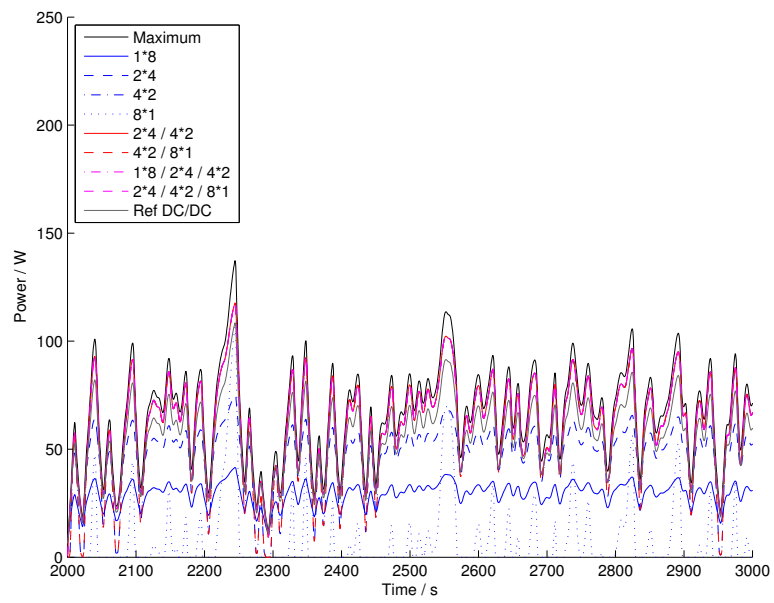


Figure G.8: Power plot for a selected time interval from the Brussels cycle, Ser/Par